Centrifugal Barrier in Low Mass Star Formation

University of Virginia
Department of Astronomy

Dylan C Jones
Advisor: Zhi-Yun Li

11 May 2021

Abstract

The classical sense of the centrifugal barrier comes from a single infalling particle at the edge of a collapsing molecular cloud core. As the particle collapses, it reaches a location, the centrifugal barrier, where it must rotate at a superkeplerian speed in order to generate a centripetal force large enough to slow down the infall speed. Within this thesis, we attempt to understand and identify this phenomenon by using hydrodynamic simulations. We present three sets of simulations exploring the parameter space of our physical model. The first set of simulations utilizes the isothermal equation of state and a $1/r^2$ initial density profile. Then a uniform density profile was used, and finally we present our reference model, a uniform density profile with the Stiffened equation of state. We find a superkeplerian rotating region near the edge of a protostellar disk in our reference model, which is similar to this classical sense of the centrifugal barrier, but differs in that the superkeplerian rotation exists because of fluid interactions necessary to slow the collapse of the infalling envelope, rather than a single infalling particle.

I. Introduction

The physical processes related to the distribution of angular momentum during star formation are not fully understood. For example, if angular momentum was fully conserved during the collapse of a rotating molecular cloud core to form a star, then we would expect collapsed material at smaller radii to be rotating significantly faster than what is observed. This problem is referred to as the 'angular momentum problem' within astrophysics and was first explored by Spitzer Jr (2008)

In the late 1970s, a series of papers including Ulrich (1976) Cassen & Moosman (1981) Shu (1977), and later Stahler et al. (1994) in the 90s, were published focusing on single particle trajectories during star formation. These papers probe into the the classical sense of the centrifugal barrier. The trajectory of an individual particle of gas can be followed as is collapses towards the protostar. As it collapses, its initial gravitational potential energy is exchanged for kinetic energy. By the time it reaches the point in which its centripetal force is balanced by the gravitational force, a location known as the centrifugal radius, it still has significant infall velocity and continues to collapse further. The particle must increase its centripetal force in order to prevent further infall. The location where this happens is referred to as the centrifugal barrier. At this point all of the available kinetic energy has been converted into rotational motion. As the core continues to collapse, material continues to pile onto this location. Piling up of material causes an increase of density, and consequently temperature, making these locations not only significant to know the mechanism for star and protostellar disk formation, but it also has application in astrochemical studies, as high temperatures and densities to a certain point aid in the formation of complex organic molecules.

As stated previously, the centrifugal barrier is the location in which all of the infall kinetic energy has been converted into rotational energy. From the definition

of angular momentum and energy conservation, we can equate the gravitational energy to rotational and infall kinetic energy.

$$\frac{m}{2}\left(v_{rot}^2 + v_{infall}^2\right) = \frac{GMm}{r} \tag{1.1}$$

At the centrifugal barrier $v_{infall} = 0$. Rearranging for v_{rot} gives us the following expression,

$$v_{rot} = \sqrt{\left(\frac{2GM}{r}\right)} \tag{1.2}$$

Writing 1.2 in terms of Keplerian velocity...

$$v_{rot} = \sqrt{2} v_{kep} \tag{1.3}$$

Equation 1.3 will be referenced within the data analysis further in this thesis as a way of identifying the location of the centrifugal barrier. Equation 1.2 can be solved for the radius at the centrifugal barrier...

$$r_{CB} = \frac{2GM}{v_{rot}^2} \tag{1.4}$$

Which can then be compared to the point in which the particle is rotating at the Keplerian speed for the first time - the centripetal force balances the gravitational force.

$$\frac{GMm}{r^2} = \frac{mv_{rot}^2}{r} \tag{1.5}$$

$$r_{CR} = \frac{GM}{v_{rot}^2} \tag{1.6}$$

When comparing equation 1.6 and 1.4, it is apparent that the radius of the centrifugal barrier is twice that of the centrifugal radius.

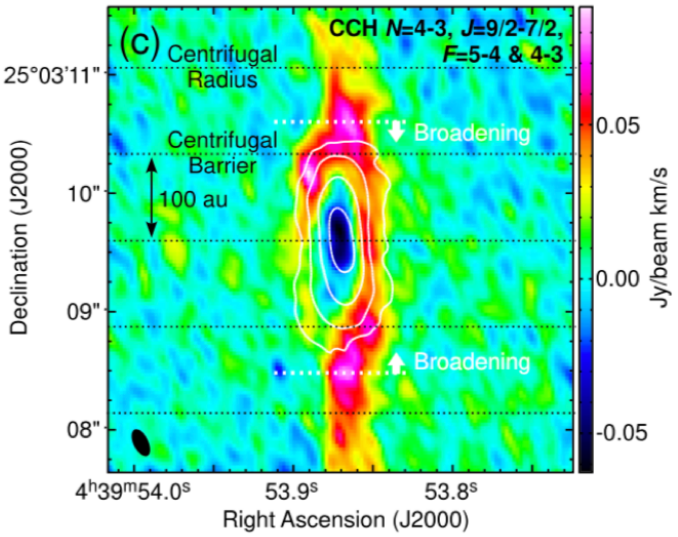

Figure 1.1: Sakai et al. (2017)

Observational confirmation for the existence of what seems to be a centrifugal barrier comes from Sakai et al. (2017) at Riken, who observed the envelope/disc system of the low-mass Class 0 protostar L1527 using ALMA. One such observation from their paper can be found in Figure 1.1. In addition to presenting observational evidence of a centrifugal barrier, Sakai reflects on limitations of the assumptions made within the classical centrifugal barrier model. The assumption that all of the available kinetic energy must be converted into rotational energy at the point of the centrifugal barrier cannot always be made, as the kinetic energy can be converted into other forms of energy such as thermal energy in the form of a shock or emitting gas. Other limitations of this classical view of the centrifugal barrier is that it disregards any effects of the magnetic field, which can drive outflow from the system, acting to reduce the specific angular momentum available.

II. Problem Setup

2.1 Governing Equations

The following two equations, derived by Euler's equations for self-gravitating hydrodynamics, are evaluated within our physical model. The first equation is the differential form of the continuity equation. The second equation is the time dependent momentum equation.

$$\frac{\partial \rho}{\partial t} + \nabla \cdot (\rho \boldsymbol{v}) = 0, \tag{2.1}$$

$$\rho \frac{\partial \boldsymbol{v}}{\partial t} + \rho \left(\boldsymbol{v} \cdot \nabla \right) \boldsymbol{v} = -\nabla P - \rho \nabla \Phi_g + \nu_0 \nabla^2 \boldsymbol{v}, \tag{2.2}$$

The gravitational potential is evaluated using the Poisson equation, which follows as

$$\nabla^2 \Phi_g = 4\pi G \rho, \tag{2.3}$$

The term $\nu_0 \nabla^2 \boldsymbol{v}$ in equation 2.2 corresponds to the viscous force. ν_0 is the dynamical viscosity, a product of the the sound speed, the disk height, and some constant alpha, given by Kuiper et al. (2010)

$$\nu_0 = \alpha c_S H \tag{2.4}$$

The disk height, H, can be written as a ratio of the sound speed to local Keplerian angular velocity, where the Keplerian angular velocity is calculated by integrating the enclosed mass of a sphere up to radius r. Finally, the dynamical viscosity is evaluated within our physical model with the following expression.

$$\nu_0 = \alpha \Omega_K(r) R^2 \left(\frac{H}{R}\right)^2 \tag{2.5}$$

The ratio $\left(\frac{H}{R}\right)$ is taken to be 1/10. The parameterization of viscosity discussed within this paper refers to this constant 'alpha', therefore the dynamical viscosity will frequently be referred to as alpha viscosity. Viscosity can also be parameterized in terms of the constant β where $\beta \approx 0.01\alpha$.

2.2 Numerical Method

The physical model presented was performed using Athena++, a grid based simulation that allows for the solving of conservative magnetohydrodynamic (MHD) equations. In this paper, we disregard the effects of the magnetic field on star formation, strictly utilizing the computational hydrodynamic capabilities of Athena++.

Our model utilizes a 2-dimensional spherical polar coordinate system, symmetric across the rotational axis. The chosen grid based model uses logarithmic spacing in the radial directions and constant spacing in the theta direction. Logarithmic spacing has the advantage of producing smaller cell sizes at smaller radial values, producing higher resolution results at radii relevant to disk formation, at the expense of producing larger cells at larger radii, which are not as critical for our analysis. Cubic cells were obtained using the logarithmic spacing scale by the following equation,

$$r = \left(\frac{x_{max}}{x_{min}}\right)^{1/n} \tag{2.6}$$

Where x_{max} and x_{min} are the range of r values in the Cartesian Coordinate system, and n is the total number of cells in the r direction. 128 cells in the r direction and 64 cells in the theta direction were used during the majority of the explorations within this paper. The resolution was increased twofold in both the r and theta directions, for a total of 256 cells in the r direction and 128 cells in the theta direction within specified 'high resolution' runs.

There are 3 boundary conditions treated within the simulation frame. The boundaries at the inner and outer edge are treated the same, assumed to be a semi-outflow boundary condition. Material is allowed to exit the computational domain but not enter back in. When the vector of the velocity is pointing outwards, the ghost zones along these boundary conditions become equivalent to the velocity and density of the last cell bordering the boundary. In this way, the velocity in the ghost zone is always pointed outwards. The boundary condition taken at the pole is treated as a reflective boundary condition, the standard boundary condition used for poles in similar simulations.

2.3 Model Setup and Parameters

We present three series of models within section 3, consisting of several different parameter explorations, concluding with a presented 'Reference Model'.

Within section 3.1, an initial density profile scaled to $1/r^2$ is used. An enclosed mass of $M_{enclosed} = 4M\odot$ and isothermal sound speed of cs = 0.2 km s^{-1} was conserved within all models.

The first presented set of simulations had an initial density profile scaled to $1/r^2$. The inner radius of these models was 10AU with an outer radius of 10,000AU. An initial solid body rotation of $\Omega = 1.189 \times 10^{-13}$ s^{-1} was used. This series of models were ran assuming an isothermal equation of state, with a temperature of $T = 10K$. A range of alpha viscosity values were utilized within one of our parameter explorations, ranging from 0-100.

The second set of models conducted had an initial constant density profile. The inner radius of these models was 2AU with an outer radius of 10,000AU. The initial solid body rotation was decreased by a factor of 2 in comparison to the $1/r^2$ exploration, with $\Omega = 5.945 \times 10^{-14}$ s^{-1}. The model was once again conducted using the isothermal equation of state with the same temperature as before. The range of alpha viscosity values conducted within this set of models was smaller, only ranging from 0-10. This set of models concluded with identified reference model parameters, as will be discussed with in section 3.2. This specific model was ran again increasing the overall resolution of the simulation, two-fold in both the r and theta directions, specified within section 2.2.

Lastly, we use the Stiffened Equation of State in order to reproduce our reference model. The Stiffened equation of state assumes an isothermal equation of state with $T = 10K$ when the density within that locality is under a specified critical density. Above this critical density, an adiabatic equation of state is used. This

critical density value was set to be 10^{-13}g cm^{-1}. The same initial constant density profile and initial solid body rotation, specified within the previous exploration, were conserved. The reference model uses an alpha viscosity = 7.

Simulations

3.1 r^{-2} Initial Density Profile

This initial density profile was chosen because it has been shown from observations that cores are centrally dense, and can be approximated with a power law scaling $\rho \approx r^{-2}$

The first set of simulations conducted explored the effect of differing alpha viscosity on disk formation. The first model had an alpha viscosity of 0. Within our physical models, without an adequate amount of viscosity, there is not an efficient mechanism to shed angular momentum as material falls inward, and this material ends up accumulating within a turbulent, self-gravitating ring, which expands outwards as the simulation progresses. The below figure illustrates a 2-dimensional depiction of this ring.

Following this ring formation, models were ran to find the viscosity in which a protostellar disk would form instead of the ring. This range included models with alpha viscosities equal to .01, 0.1, 0.3, 3.0, and 10.0.

The lowest viscosity model once again formed a ring. The turbulent nature observed prior with the 0 viscosity case was observed again with this simulation. It was found that increasing the alpha viscosity eventually transitions this ring into an intermediate between a disk and a ring. The increased viscosity also acted to prevent the turbulent nature seen previously. Above alpha viscosities = 0.1 or so, a self-gravitating disk forms, which grows in size as the simulation continues. Egregiously high viscosity values greater than 10 resulted in quick accretion of the gas material into the inner boundaries because of the efficiency of the transfer of angular momentum within the protostellar disk. Figure 3.2 illustrates the different

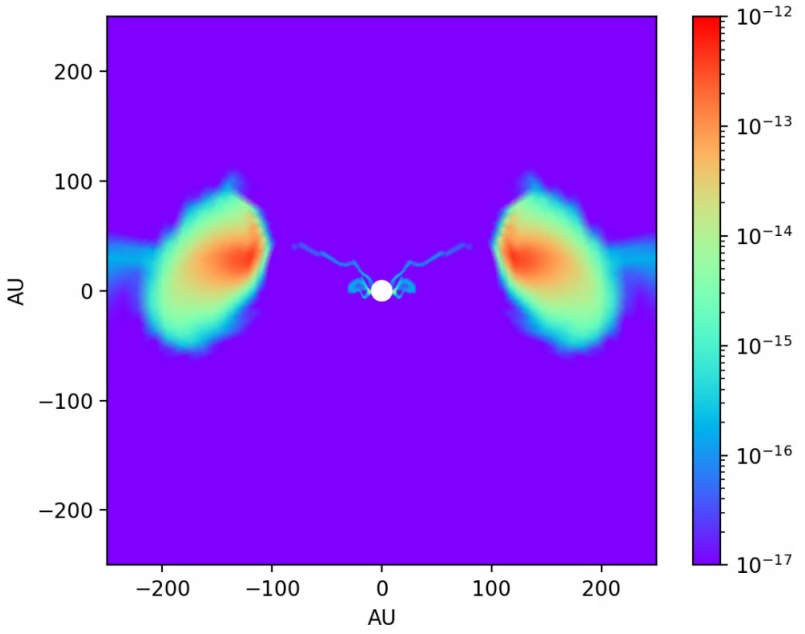

Figure 3.1: Density map for the viscosity = 0 simulation. The density colorbar is in units $\mathrm{g\,cm^{-1}}$

stages of disk or ring formation for several alpha viscosity values in terms of density, infall, and radial velocity at various times. These data values are gathered from the midplane of the simulation.

All of the models began with the prescribed initial density distribution, decreasing with a power law, starting with $\rho \approx 10^{-14}\mathrm{g\,cm^{-1}}$ at the inner boundary of 10 AU to $\rho \approx 10^{-20}\mathrm{g\,cm^{-1}}$ at the outer boundary of 10,000 AU. There is initially no infall velocity, but there is some initial solid body rotation specified within section 2.2. As time progresses, material closer to the inner edge of the simulation begins to fall inwards and rotate faster until $\approx t = 50,000 years$, when the first rotationally supported structures form. This time frame can be seen within Figure 3. The density at smaller radii are orders of magnitude larger than the density outside of this structure. The infall velocity of $v_i \approx 0\mathrm{km\,s^{-1}}$ is also indicative of this rotationally supported structure - material at these radii is supported by its centripetal force against the gravitational force exerted by the protostar.

Past these initial frames, the behavior of each model becomes more distinct. A 1-dimensional depiction of Figure 3.1, along the midplane, can be found within Figure 3.2c. This time of t = 100,000 years is still relatively early within the simulation, thus there is still material at the smaller radii, albeit considerably less than the other viscosity simulations. This material is not falling inwards, but

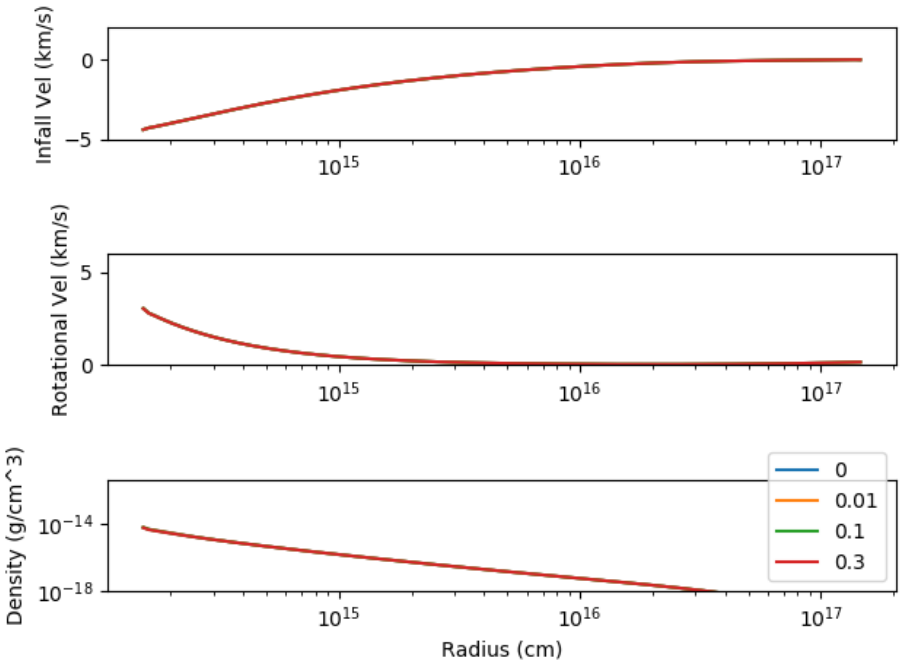

(a) t = 30,000 years

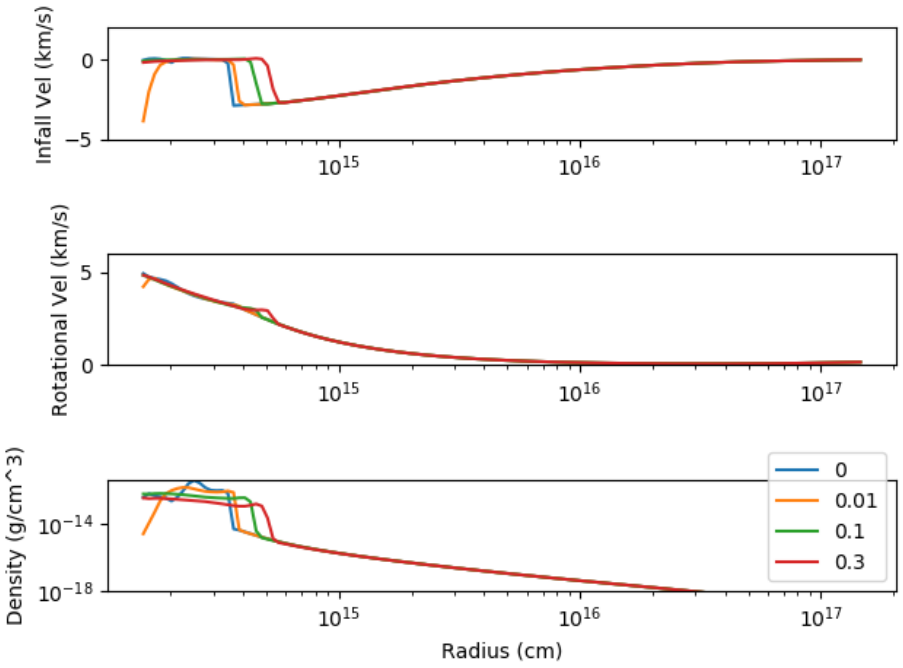

(b) t = 50,000 years

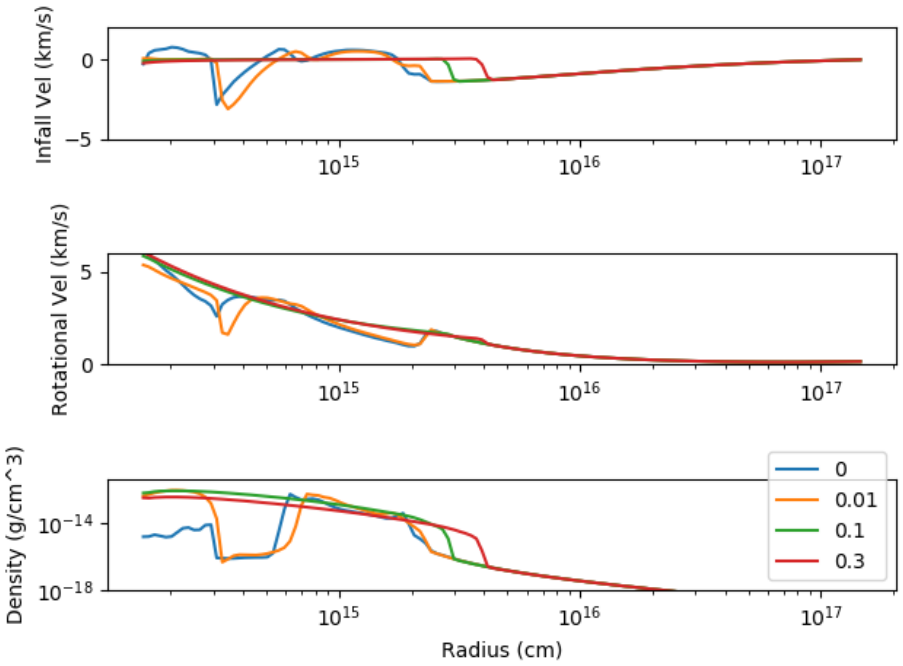

(c) t = 100,000 years

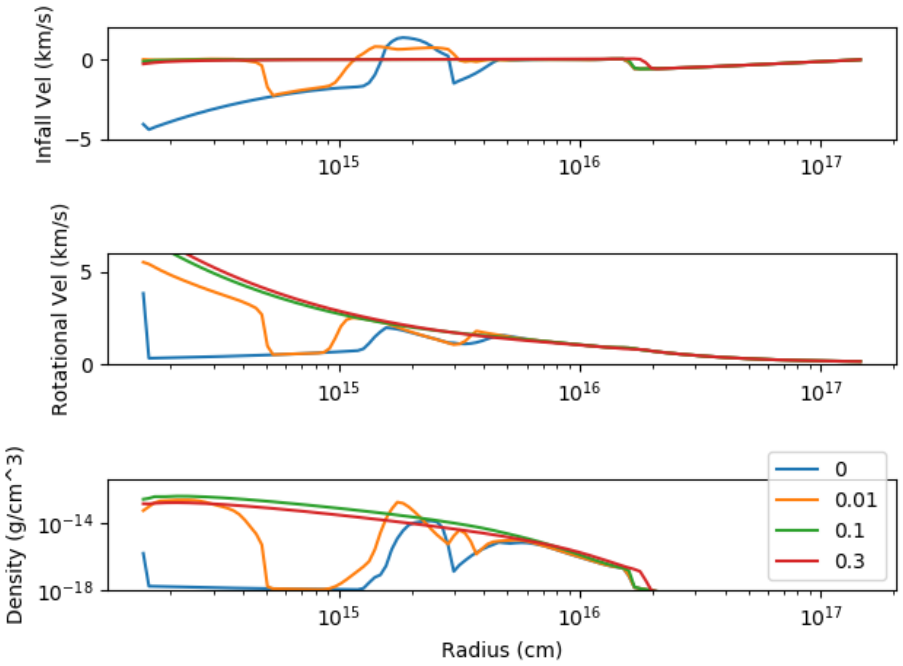

(d) t = 210,000 years

Figure 3.2: Infall velocity, rotational velocity, and density along the midplane of the above described models. A negative infall velocity indicates material that is moving inwards, towards the center of the simulation.

rather moving outwards due to its high rotational velocity. The ring structure itself starts at $r \approx 4 \times 10^{14} cm$ and ends around $r = 1 \times 10^{15} cm$. Within this radius range, the density of the ring is comparable to the other simulations. The next lowest viscosity simulation has an alpha viscosity = 0.01. At this time frame, the intermediate nature of the lower viscosity values can begin to be observed. At smaller radii, it has comparable densities to that of the higher viscosity simulations. It differs from the 0 viscosity model at these small radii in that it is not expanding outwards, the infall velocity within this range is 0. However, past 20AU, there is a significant decrease in density, matched by an increased in infall velocity towards the center of the simulation. This density decrease continues until 80AU, where the density increases exponentially and more-so matches that of the remainder of the simulations. Finally, the behavior of the alpha viscosity simulations equal to 0.1 and 0.3 are very similar. A rotationally supported structure forms on the order of 110-120AU.

The last provided figure for this viscosity exploration occurs at a time t = 210,000 years. The ring at this time frame is more pronounced, with low densities at lower radii and a large increase in density starting at r=100AU. This hump at 100AU is extremely turbulent and will increase or decrease in size by 5-10AU between two adjacent time frames. The alpha viscosity equivalent to 0.01 shares this behavior with its equivalent hump at around 100AU. Both the 0 viscosity and 0.01 viscosity have a structure that follows closely to the protostellar disks of the other simulations between 300-1,000AU that grows in size outwards for the remainder of the simulation. At this point within the model, the higher viscosity cases simply grow outwards with time, no other additional behavior as seen with the smaller viscosity cases is noted.

As discussed in section 1, identification of the centrifugal barrier can occur by comparing the local Keplerian velocity to rotational velocity. The local Keplerian velocity was calculated at every r,theta value within the simulation. The ratio of rotational velocity to local Keplerian velocity, as a function of radius, along the midplane of the simulation, was then obtained.

In the previously presented series of models, this ratio was obtained for each outputted time step. It was generally seen, that prior to disk formation (which occurs $t \approx 50{,}000$ years) the ratio increases stronger at smaller radii than at larger radii. The value of the ratio increases until a value of 1.4 is reached at the inner edge of the simulation, every time prior to formation of a protostellar disk. Once this value was reached, a Keplerian rotating disk propagates outwards for the remainder of the simulation. This once again supports the claim that the disks formed within these simulations are rotationally supported.

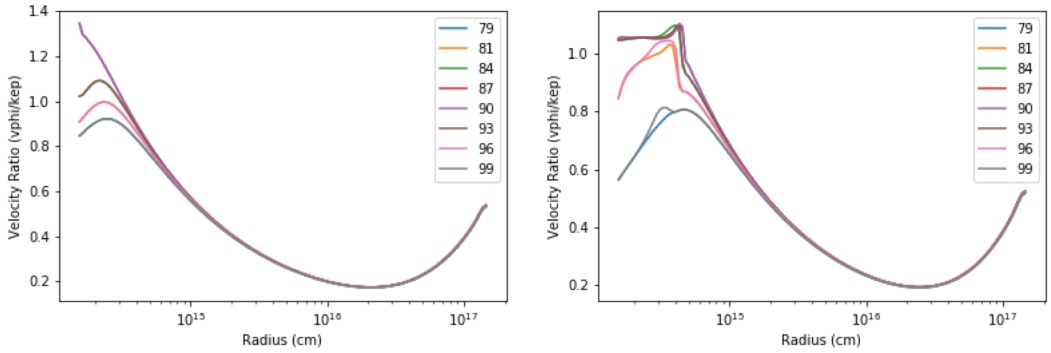

Figure 3.3: Ratio of the rotational velocity to the Keplerian velocity at time = 40,000 years (left) and time = 50,000 years (right). The legend in this plot corresponds to the angle θ the data was obtained from. The angle is taken from the rotational axis, making 90 degrees the midplane of the simulation.

3.2 Initial Uniform Density Profile

Following the viscosity explorations of the previous section, the effect of the initial density profile had on the identification of the centrifugal barrier was studied. This initial density profile was changed from the r^{-2} profile to a constant density profile. A new viscosity exploration was repeated with the identical viscosity values used within section 3.1.

It was found that the lower viscosity cases which would have formed a disk, or disk-like structure, in the previous r^{-2} density profile tends to form rings under this constant initial density profile. With angular momentum scaling to $L = mvr$, it can be seen that with a uniform density sphere, there will be higher angular momentum at larger radii in comparison to the previous density profile. A more efficient mechanism is needed to shed angular momentum so that infalling material does not clump up within a ring, but rather form a rotationally supported disk. Keeping the other parameters constant, since angular momentum also scales with rotational velocity, the initial solid body rotation Ω was reduced by a factor of two from $\Omega = 1.189 \times 10^{-13}$ s^{-1} to $\Omega = 5.945 \times 10^{-14}$ s^{-1}.

After reducing the angular momentum within the simulation, the same viscosity exploration done within section 3.1 was conducted. However, it was quickly found that within the lower viscosity values that would form a disk in the r^{-2} density

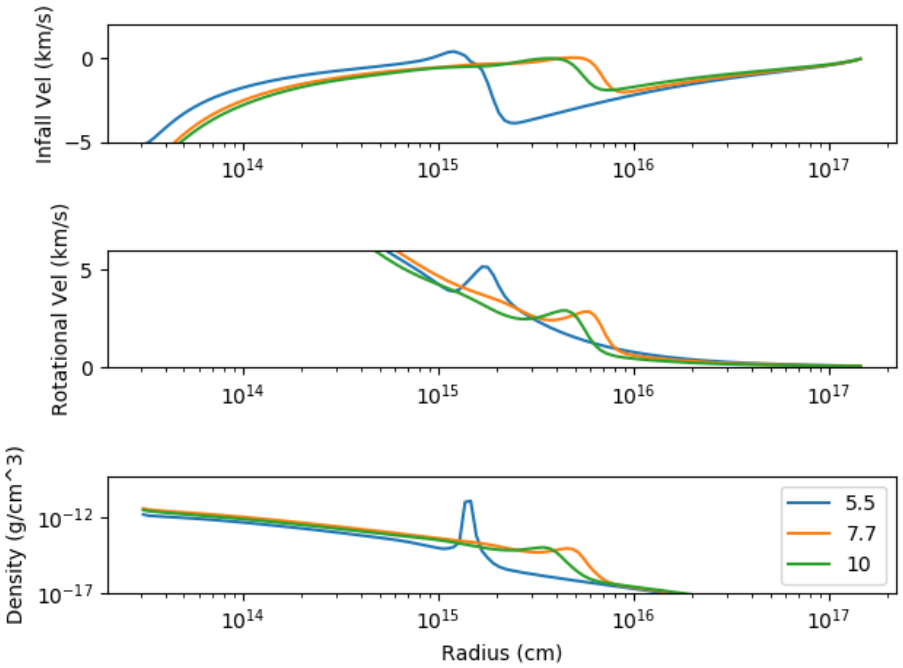

(a) Time = 110,000 years

profile still formed ring after this reduced initial solid body rotation. A smaller viscosity regime was identified along the transition between ring and protostellar disk in order to identify the lowest possible alpha viscosity that would allow a disk to form. This alpha viscosity range included 5.5, 7.7, to 10.0. Additionally, the inner boundary was decreased to 2AU. The following plot illustrates the evolution of density, rotational velocity, and infall velocity along the midplane much like Figure 3.3, but with one time frame at 110,000 years.

In the 5.5 alpha viscosity simulation, a high density ring of magnitude $\rho = 10^{-9}\mathrm{g\,cm^{-1}}$ forms around $t \approx 90,000 years$ initially at the inner edge of the simulation. A similar behavior found within section 3.1 is observed for this simulation, as it exhibits characteristics of both a ring and a disk. As the simulation progresses, material at smaller radii accumulates into a turbulent, unstable ring. Interestingly enough, the ring moves towards smaller radii as the simulation progresses, rather than outwards. The disk like structure, identified by the 0 infall velocity and density hump progresses outwards for the remainder of the simulation.

The 7.7 and 10 viscosity simulations are the ones that are able to form a rotationally supported disk. This disk forms first within the 7.7 viscosity simulation,

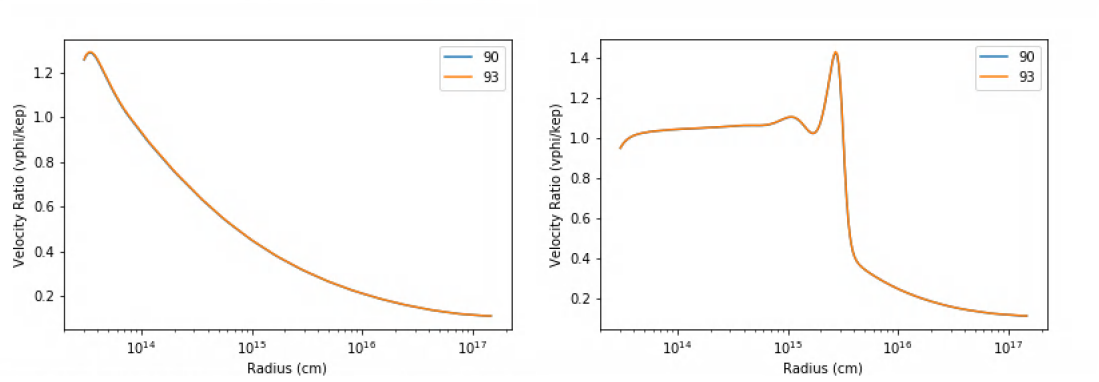

Figure 3.5: Ratio of the rotational velocity to the Keplerian velocity at time = 106,000 years (left) and time = 110,000 years (right). The legend in this plot corresponds to the angle θ the data was obtained from. The angle is taken from the rotational axis, making 90 degrees the midplane of the simulation.

at t = 81,000 years with a density of $\rho \approx 10^{-17}\mathrm{g\,cm^{-1}}$. It is not until t = 84,000 years that the 10 viscosity simulation is able to form a disk at a radius of 25AU, while the 7.7 viscosity simulation already has evolved a disk to $\approx 75AU$. This lag in terms of disk size in comparison to simulation time remains for the remainder of the model.

The difference between the 7.7 and 10 viscosity simulations is additionally interesting when looking at the plots of the ratio of rotational velocity to local Keplerian velocity. As found in the previous section, we still find that this ratio reaches a value equal to 1.4 prior to disk formation. Further we find that for the 7.7 viscosity simulation, there exists a sharp hump along the disk edge equivalent to this ratio of 1.4 which grows with the protostellar disk for the remainder of the simulation. The disk remains a Keplerian rotating structure. The higher viscosity case does not reach this value of 1.4. Rather, a superkeplerian value of 1.2 is maintained along the disk edge for the remainder of the simulation. Because of this finding, the viscosity value of 7.7 was chosen to be the fiducial value to be tested within the section.

Within Figure 3.5, the rotational speed meets the Keplerian speed at a radius of around. $r = 2 \times 10^{16} cm$. The location of the local maximum occurs at a radius of $r = 1.5 \times 10^{16} cm$. These locations differ from the classical sense of the centrifugal barrier where the location of the centrifugal radius, where the rotational speed is equivalent to Keplerian speed is at a radius twice as far as the centrifugal barrier,

the location where the ratio of these two velocities is 1.4.

3.3 Reference Model, Stiffened EOS

The fiducial parameters to be used within the Stiffened equation of state were established using the isothermal equation of state. The disk that forms with these parameters is above the critical density of $\rho = 10^{-13}\mathrm{g\,cm^{-1}}$, therefore it is apparent that the adiabatic equation of state will play some role in disk formation at densities above such values.

The model begins with a 90,000 year collapse. Immediately after the collapse, a thermally-supported first core with a radius of 20AU at 91,000 years forms. Following the first core, a rotationally supported disk forms which grows in radius with time for the remainder of the simulation. At time 98,000 years, we form a disk with the radius on the order of 150AU. This progression within our reference model can be seen within the sequence of density plots in Figure 3.6.

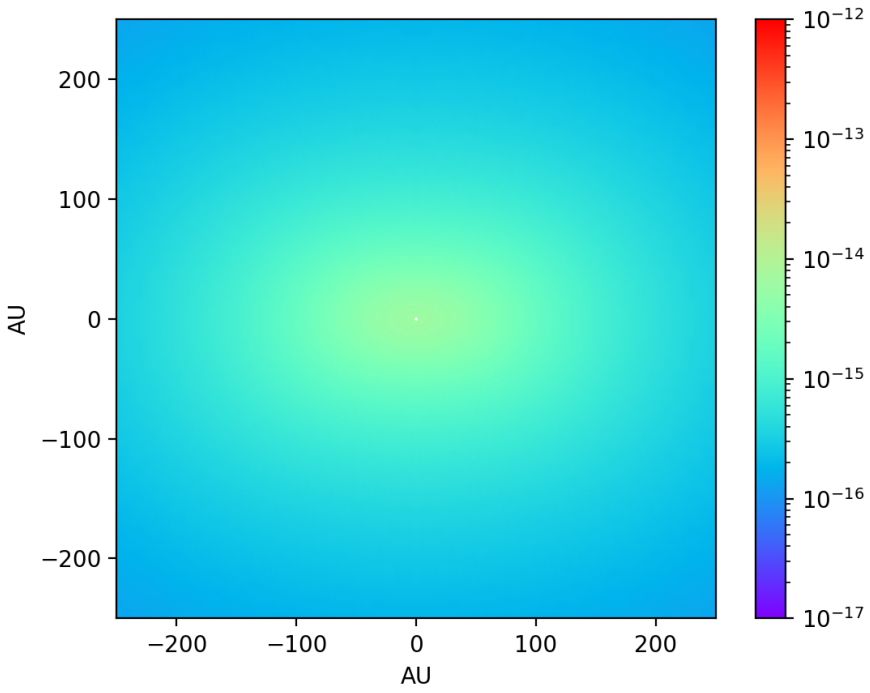

(a) time = 90,000 years

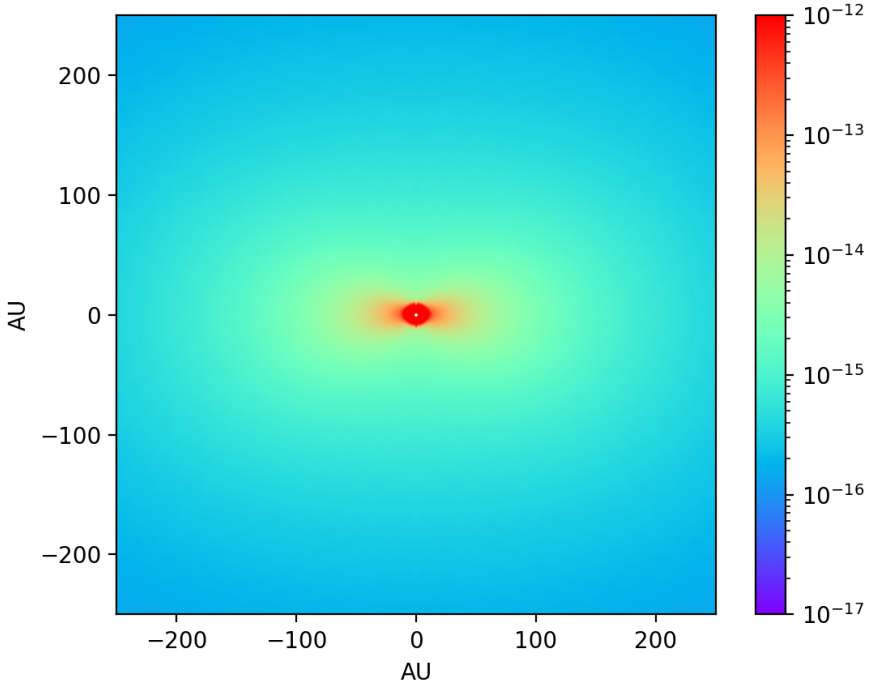

(b) time = 91,000 years

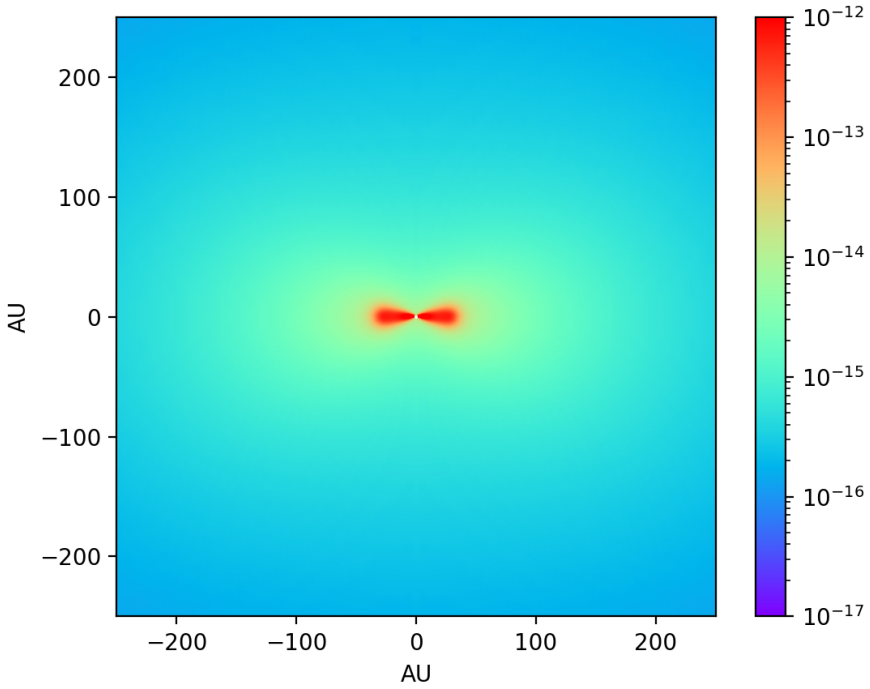

(c) time = 92,000 years

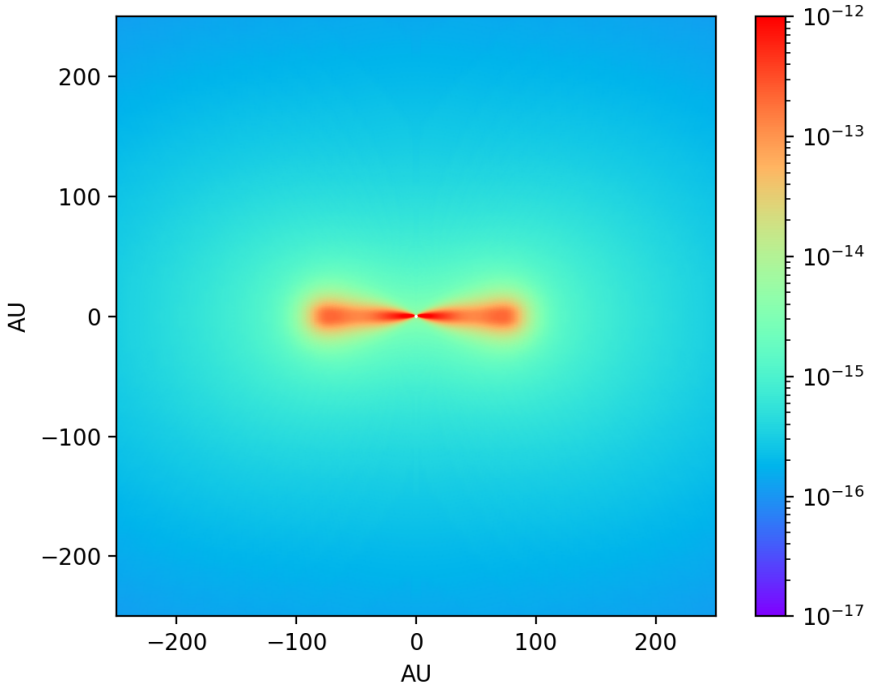

(d) time = 95,000 years

Figure 3.6: Density Maps for our Reference Model. The scale of the colorbar is in $\mathrm{g\,cm^{-1}}$

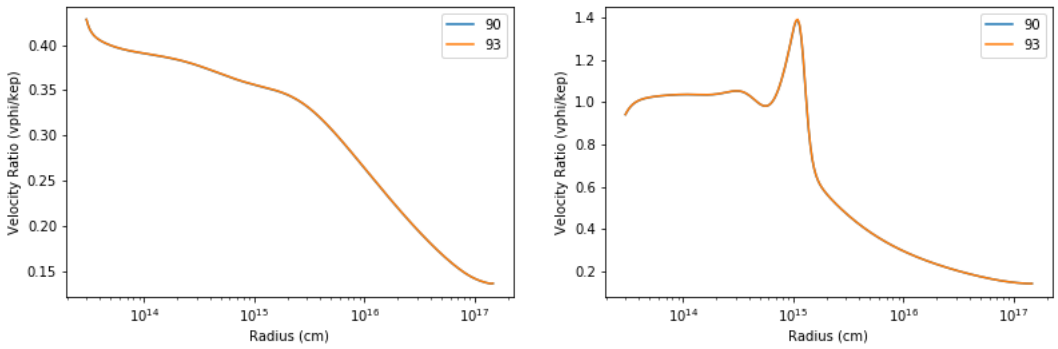

Figure 3.7: Ratio of the rotational velocity to the Keplerian velocity at time = 90,000 years (left) and at 94,000 years (right)

The analysis of the density plots for this simulation does not necessarily distinguish it from the isothermal equation of state. An analysis of the rotational to Keplerian velocity reveals that disk formation is not preceded by the ratio of this value reaching 1.4 along the inner boundary of the simulation, as was the case in the isothermal simulations. Instead, the thermopressure gradient acts to erase this phenomenon. The characteristic hump found along the edge of the disk, reaching a maximum value of 1.4 is still found while using the Stiffened equation of state. The following two figures illustrate this ratio before and after disk formation. Looking at the locations of the centrifugal radius and barrier within Figure 3.5 shows that these radii are not a factor of two apart, consistent with the isothermal simulations.

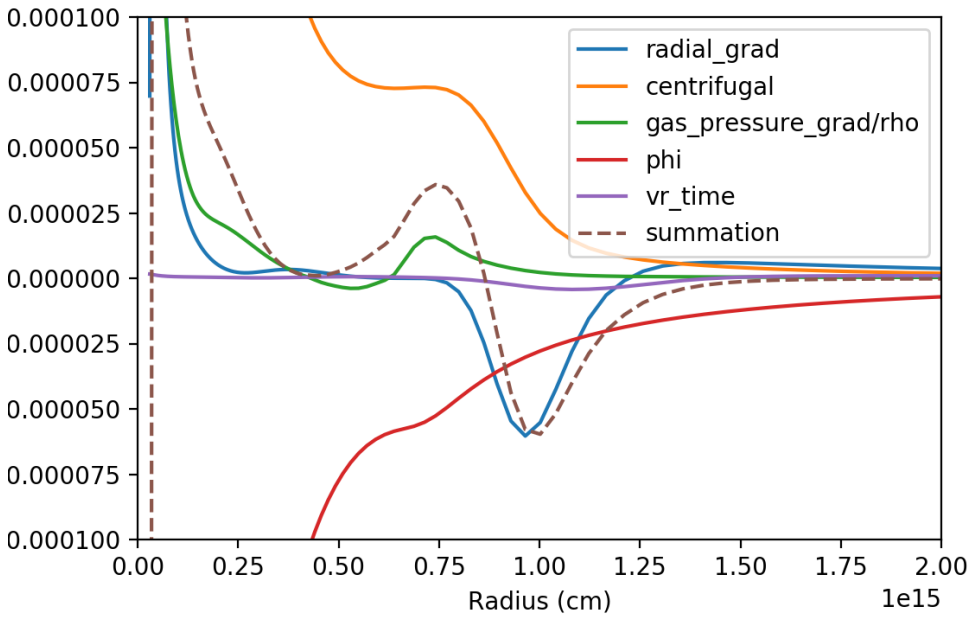

Figure 3.8: Force terms from equation 2.2. Units of the y scale is in gcm^3s^{-1} It should be noted that since the dt of the simulation was too large, the time derivative of radial velocity is not significantly accurate. Time = 93,000 years.

Further analysis of this simulation is possible by plotting the different forces involved in equation 2.2.

A Keplerian rotating particle would have a $1/r^2$ profile for its centripetal force (orange line). Within this figure, there is a bump along this orange line which corresponds to the superkeplerian rotating region in Figure 3.7b. Around $0.33 \times 10^{15} cm$ from the peak on this graph is a significant minimum in the radial gradient, corresponding to a large deceleration of material at that location. This is likely from the infalling material accreting onto the envelope. If we mark $1 \times 10^{15} cm$ as the edge of the disk, then the superkeplerian region is disk material, not the infalling material, proving to be one derivation from the classical sense of the centrifugal barrier. We tentatively conclude that the envelope material must spin up to this superkeplerian speed in order to slow down the collapsing envelope onto the disk.

Conclusion

In summary, we have used Athena++ to perform conservative hydrodynamic simulations of the formation of low mass stars in an attempt to reproduce and understand the concept of the Centrifugal Barrier.

The first portion of this exploration was performed with an initial density profile scaled to a power law of $1/r^2$ with an isothermal equation of state. Within this set of simulations, we find that when viscosity is absent from the simulation, material tends to clump together and form a ring. The addition of viscosity to the simulation allows this ring to transform into an intermediate between a ring and a protostellar disk, and when the viscosity is high enough, a disk. Along the inner boundary of these simulations, we found that prior to the formation of the disk, the material at small radii must reach a value of this ratio between rotational velocity and Keplerian velocity equivalent to 1.4.

Next, we presented a set of simulations assuming a constant initial density profile. Because of this density profile, there is too much angular momentum in the simulation with to form a disk with the parameters from Section 3.1. For a disk to form, we reduced this angular momentum by lowering the initial solid body rotation was reduced by a factor of 2. As in the previous section, a viscosity regime transitioning from a ring to disk was identified. When plotting this ratio of rotational velocity to Keplerian velocity as a function of radius, we find that in the viscosity = 7.7 simulation, material reaches this ratio value equal to 1.4 near the outer edge of a Keplerian rotating disk.

The fiducial parameters found in Section 3.2 were ran using the stiffened equation of state for our Reference Model. After a 90,000 year collapse, we form a thermally supported first core, which flattens out to form a ring. The superkeplerian initialization condition from the isothermal explorations was found to be an artifact

of that equation of state, as it is erased by the thermopressure gradient with the stiffened equation of state. The superkeplerian hump found within Section 3.2 still occurs.

In our simulation, we have found something that is similar to the centrifugal barrier, identified by a superkeplerian rotating structure with the rotational velocity $\sqrt{2}$ higher than the Keplerian velocity near the outer edge of the disk. However, this structure differs from the classical sense of the centrifugal barrier outlined within the introduction. We found that the centrifugal radius, the point in which the rotational velocity is equivalent to the Keplerian velocity for the first time, does not occur at a radius twice that of what we identify to be the centrifugal barrier. Our tentative conclusion from the reference model is that the material at the centrifugal barrier is actually part of the disk. The material here needs to rotate at a superkeplerian velocity in order to generate enough of a centripetal force to slow down of the infalling envelope. In the classical picture, the single infalling particle has to slow down without the interaction of other particles, requiring its centripetal force to be large enough to slow down its free fall speed, our presented models support a more hydrodynamic concept of the centrifugal barrier where the superkeplerian portion is not required for the slow down of the individual particle, but rather necessary to support and slow down the infalling envelope.

Acknowledgements

I would like to thank Ka Ho (Andy) Lam for working with me this past year and a half on this project. He has provided valuable insight on how Athena ++ works and has been an excellent source of knowledge whenever I encountered an issue with coding or working with the models. I would also like to thank my advisor, Professor Li, for guiding me through this project and helping with the data analysis.

Bibliography

Cassen, P., & Moosman, A. 1981, Icarus, 48, 353

Kuiper, R., Klahr, H., Beuther, H., & Henning, T. 2010, The Astrophysical Journal, 722, 1556

Sakai, N., Oya, Y., Higuchi, A. E., et al. 2017, Monthly Notices of the Royal Astronomical Society: Letters, 467, L76

Shu, F. H. 1977, The Astrophysical Journal, 214, 488

Spitzer Jr, L. 2008, Physical processes in the interstellar medium (John Wiley & Sons)

Stahler, S. W., Korycansky, D., Brothers, M. J., & Touma, J. 1994, The Astrophysical Journal, 431, 341

Ulrich, R. K. 1976, The Astrophysical Journal, 210, 377